Southern African crustal evolution and composition: Constraints from receiver function studies

Shaji K. Nair,[1] Stephen S. Gao,[1] Kelly H. Liu,[1] and Paul G. Silver[2]

[1]   Stacking of approximately 1500 radial receiver functions recorded at about 80 broadband seismic stations deployed in southern Africa reveals systematic spatial variations in the ratio of crustal P and S wave velocities (ϕ), crustal thickness (H), and the amplitude of the converted Moho phases (R). The eastern Zimbabwe and the southern Kaapvaal cratons are characterized by small H ($\sim$38 km), small ϕ ($\sim$1.73), and large R ($\sim$0.15) values, suggesting that the relatively undisturbed Archean crust beneath southern Africa is separated from the mantle by a sharp Moho and is felsic in composition. The Limpopo belt, which was created by a collisional event at 2.7 Ga, displays large H ($\sim$43 km) but similar ϕ and R values relative to the cratonic areas. The Bushveld Mafic Intrusion Complex and its surrounding areas show large ϕ ($\sim$1.78), large H ($\sim$43 km), and small R ($\sim$0.11) values, reflecting the intrusion of mafic material into the original crust as a result of the Bushveld event at 2.05 Ga. Excluding the Bushveld, the spatially consistent and age-independent low ϕ accentuate the difference between felsic crustal composition and more mafic island arcs that are thought to be the likely source of continental material. Within such an island arc model, our data, combined with xenolith data excluding mantle delamination in cratonic environments, suggest that the modification to a felsic composition (e.g., by the partial melting of basalt and removal of residue by delamination) is restricted to have occurred during the collision between the arcs and the continent.

1.   Introduction

[2]   Numerous studies during the past several decades have confirmed that the present-day continental crust is andesitic in composition, formed by island arc accretion, continental rifting, arc magmatism, continent-continent collision, and basaltic volcanism at hot spots. Whether those processes were also the dominant processes for crustal formation in the first few billion years still remains as one of the most significant unsolved questions facing geoscientists [*Griffin and O'Reilly*, 1987; *Clarke and Silver*, 1993; *Rudnick and Fountain*, 1995; *Rudnick*, 1995].

[3]   Arguably the most important piece of information in understanding continent formation is the composition of the crust of different ages, something which remains poorly known. Southern Africa (Figure 1) contains some of the largest intact terrains of Neo- and Meso-Archean ages, as well as an abundance of lower crustal granulite xenoliths. The unique geological history and setting, together with the recently acquired high-quality seismological and petrological data sets, make this area an ideal locale for studying the evolution and composition of early crust.

1.1.   Geological Background

[4]   The region covered by the seismic stations has a total area of about 1.2×10^6 km^2 (Figure 1), consisting of a number of crustal terrains with a large span of ages [*de Wit et al.*, 1992]. In the northern part of the region is the Archean Zimbabwe craton, which was formed and stablized between 2.7 and 3.0 Ga. The bulk of the study area is within the Kaapvaal craton. The Meso-Archean (2.0–3.7 Ga) crust is exposed only on the eastern side of the craton, which is separated from the Neo-Archean (2.5–3.0 Ga) western side by a NNE trending strike-slip/thrust belt. In the northern part of the Kaapvaal craton, near latitude 25°S, is the 2.05 Ga Bushveld Complex, the largest layered mafic igneous intrusion in the world. Between the Zimbabwe and Kaapvaal cratons lies the Limpopo belt, which was formed as a result of a collision between these two cratons at around 2.7 Ga. The southernmost part of the study area consists of the Proterozoic (1.1–1.9 Ga) Namaqua-Natal mobile belt and the Paleozoic (about 0.3 Ga) Cape Foldbelt [*de Wit et al.*, 1992; *Tankard et al.*, 1982; *de Beer and Stettler*, 1988; *de Wit and Roering*, 1990].

1.2. V_p/V_s Ratio and Its Implications

[5]   The P and S wave velocity ratio, $\phi = V_p/V_s$, which is closely related to the better known Poisson's ratio by $\sigma = 0.5[1 - 1/(\phi^2 - 1)]$, provides much tighter constraints on crustal composition than either the P or S wave velocity alone [*Tarkov and Vavakin*, 1982; *Christensen*, 1996;

[1]Geophysics Group, Kansas State University, Manhattan, Kansas, USA.
[2]Department of Terrestrial Magnetism, Carnegie Institution of Washington, D. C., USA.
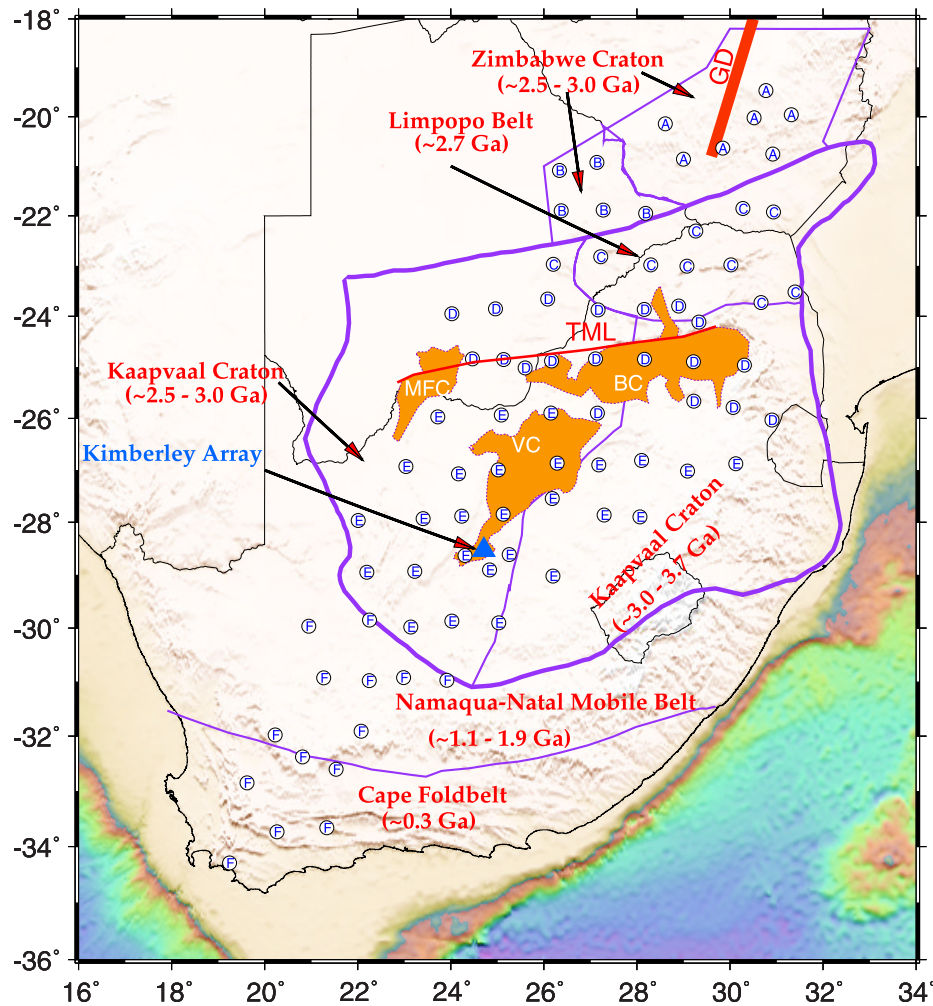
Figure 1. A topographic map showing the major geologic provinces and their ages, and distribution of seismic stations (open circles) used in the study. The triangle represents the Kimberley Array. The letter in the open circles is the tectonic area to which the station belongs: A, eastern Zimbabwe craton; B, western Zimbabwe craton; C, Limpopo belt; D, Bushveld Complex and vicinity; E, southern Kaapvaal craton; F, post-Archean fold belts. All the stations were equipped with broadband, three-component sensors. The seismograms were interpolated to a uniform rate of 20 samples per second. GD, Great Dike; MFC, Molopo Farms Complex; BC, Bushveld Complex; VC, Ventersdorp Complex; TML, Thabazimbi-Murchison Lineament.

Chevrot and van der Hilst, 2000]. Laboratory measurements suggest that variations in ϕ are due primarily to SiO_2 content [*Tarkov and Vavakin*, 1982] with a more mafic crust corresponding to a higher value of ϕ [*Christensen*, 1996]. Those measurements also show that ϕ does not vary significantly with pressure or temperature. The relative abundance of quartz ($\phi = 1.49$) and plagioclase ($\phi = 1.87$) has a dominant effect on the ϕ of common igneous rocks or their metamorphosed equivalents [*Christensen*, 1996]. Both an increase in plagioclase content and a decrease in SiO_2 content lead to an increase in ϕ. For instance, a granitic rock has a ϕ of 1.71; for a diorite, $\phi = 1.78$; and for a gabbro, $\phi = 1.87$ [*Tarkov and Vavakin*, 1982]. Laboratory experiments on likely compositions at crustal P,T conditions suggest that ϕ varies from 1.74 in the upper crust to 1.81 in the lowermost crust, which leads to a mean crustal ϕ of 1.78 [*Christensen*, 1996].

1.3. Previous V_p/V_s Ratio Measurements

[6] Recognizing the potential importance of ϕ in constraining crustal composition, there has been extensive work on estimating this parameter. There have been several receiver-function-based studies using $P\acute{m}S - P$ and $PP\acute{m}S - P$ (using the terminology of *Clarke and Silver* [1991]) differential travel times. *Zandt and Ammon* [1995] measured ϕ at 76 sites worldwide. They found the highest mean ϕ (1.84 ± 0.06) for Precambrian shields, intermediate (1.78 ± 0.06) for Proterozoic platforms, and the lowest (1.73 ± 0.09) for Cenozoic and Mesozoic crust, suggesting that ϕ increases with the age of the crust. Given the stated uncertainties, however, this apparent age dependence is only marginally significant. Indeed, this observation, especially the high ϕ for Archean crust, appears to be inconsistent with several petrological and seismological studies, which suggested that the Archean crust is, on average, less mafic than the

post-Archean crust, because it lacks a high-velocity, presumably mafic, lower crust [*Durrheim and Mooney*, 1994; *Griffin and O'Reilly*, 1987].

[7] Beneath North America, a combination of averaged crustal shear wave velocities from surface waves with compressional wave velocities at 64 sites resulted in an average crustal ϕ of 1.75 ± 0.13 [*Braile et al.*, 1989]. *Clarke and Silver* [1993] found that ϕ ranges from 1.67 to 2.08 under six stations in North America. *Zandt et al.* [1995] presented measurements along a 200-km-long transect across the eastern Basin and Range and western Colorado Plateau at 37° latitude, and found that the western Colorado Plateau crust is characterized by a high ϕ (1.81–1.84). They interpreted the high ϕ as being the indication of a crust with an average mafic composition. In southern California, *Zhu and Kanamori* [2000] found an average ϕ of 1.78, with higher values of 1.80 to 1.85 in the mountain ranges with Mesozoic basement.

[8] *Owens and Zandt* [1997] measured crustal thickness (H) and ϕ across the Tibetan plateau using shear-coupled teleseismic P waves from a deep earthquake, which revealed a northward thinning of the crust and an increase in ϕ, from about 1.78 to 1.99, which they explained by partial melting of the lower crust beneath northern Tibet. A more recent study [*Kind et al.*, 2002], however, found no substantial regional difference in crustal ϕ between northern and southern Tibet.

[9] Measurements of ϕ obtained along Deep Seismic Sounding (DSS) profiles in the former Soviet Union revealed a ϕ of about 1.727 for cratons, 1.735 for Paleozoic fold belts, and 1.716 for Cenozoic basins [*Egorkin*, 1998]. Beneath the cratons, ϕ is found to be positively correlated with H, and the opposite is found for the other two types of areas.

[10] Using data from 28 broadband seismic stations, *Chevrot and van der Hilst* [2000] found a mean ϕ of 1.79 for the western Australian Archean crust, 1.76 for the central Proterozoic crust, and 1.75 for the eastern Phanerozoic crust (calculated based on Table 1 of *Chevrot and van der Hilst* [2000]). They also found that inside the Proterozoic domains, ϕ tends to increase with increasing H, which was explained as an increase of the thickness of a mafic lower crust. In the Phanerozoic provinces, however, ϕ tends to decrease with increasing H.

[11] On the basis of the highly variable results presented in these previous studies, there appears to be no clear-cut relationship between ϕ and other physical variables, such as age or thickness of the crust. Some studies have suggested that Archean crust has high ϕ, but these relationships remain weak, in our opinion, and probably within the uncertainty in the data. The results of *Chevrot and van der Hilst* [2000], while arguing for two separate relationships between ϕ and H, could be fit equally well by a bimodal distribution of ϕ that is independent of either age or crustal thickness.

1.4. Recent Seismic Studies of Southern African Crust

[12] The multidisciplinary Southern African Seismic Experiment (SASE) consisted of a large array of 55 broadband seismographs spanning a large portion of southern Africa (Figure 1) during a 2-year period that occupied a total of 82 sites. The area covered by the stations is about 2000×600 km^2. Embedded within this array is a much smaller experiment (i.e., the Kimberley array), which covered a 60×40 km^2 area using 32 broadband stations in the diamondiferous southern Kaapvaal craton near the city of Kimberley for a 6-month period [*Niu and James*, 2002]. The current study uses data from the larger array, which covered an area that is about 400 times larger than that covered by the Kimberley array (Figure 1).

[13] Crustal thickness at most of the 82 stations has been measured by several studies [e.g., *Nguuri et al.*, 2001; *Stankiewicz et al.*, 2002]. Despite disagreements of up to several km for some of the stations between those studies, virtually all of the studies suggested significant and systematic variations in H between Archean terrains that have been stable since 2.9 Ga, and younger terrains that have been subject to subsequent collisional and/or magmatic activity. In particular, the undisturbed parts of the Archean Kaapvaal and Zimbabwe cratons show thin (35–40 km) crust, while the Limpopo continental collision zone, the Bushveld Mafic Intrusion Complex, and the post-Archean fold belts south of the Kaapvaal craton were all found to have thick (45–50 km) crust.

[14] With respect to studies of ϕ in southern Africa, using data from a nearby earthquake recorded by the Kimberley array stations (Figure 1), *Niu and James* [2002] found an average ϕ of 1.73 using a modified receiver function methodology, which together with estimated lower crust density, suggests a felsic to intermediate lower crustal composition. *Stankiewicz et al.* [2002] used receiver functions from three earthquakes recorded by the Kimberley array, but the results were somewhat variable, with one event giving $\phi = 1.74$, while two events produced higher values of 1.78. This variability suggests uncertainties of order 0.05 in ϕ. The present study extends the measurements of ϕ to the entire area covered by SASE.

2. Data

[15] The data set used in the study was recorded by the 82 stations of SASE. It has been used to study various aspects of the crust and mantle beneath southern Africa, such as seismic anisotropy using shear wave splitting [*Silver et al.*, 2001, 2004], body wave velocity structure [*James et al.*, 2001], crustal thickness using receiver functions [*Nguuri et al.*, 2001; *Stankiewicz et al.*, 2002], surface wave tomography [*Freybourger et al.*, 2001], and spatial variation of mantle discontinuities from stacking of P-to-S converted phases [*Gao et al.*, 2002; *Shen and Blum*, 2003; *Niu et al.*, 2004].

[16] The data set consists of approximately 3700 three-component seismograms with observable P wave arrivals, in the epicentral distance range of 30° to 95°. In this study, the seismograms were filtered in the 0.05–1.5 Hz frequency band and were converted into radial receiver functions using the procedure of *Ammon et al.* [1990]. The receiver functions were then examined visually and those with a clear first P arrival are used in the study. A total of 1544 radial receiver functions from 88 teleseismic events were chosen (Figure 2).

[17] In Figure 3 the receiver functions are grouped into one-degree bins according to their depth-corrected epicentral distances, and those in the same bins are then stacked in
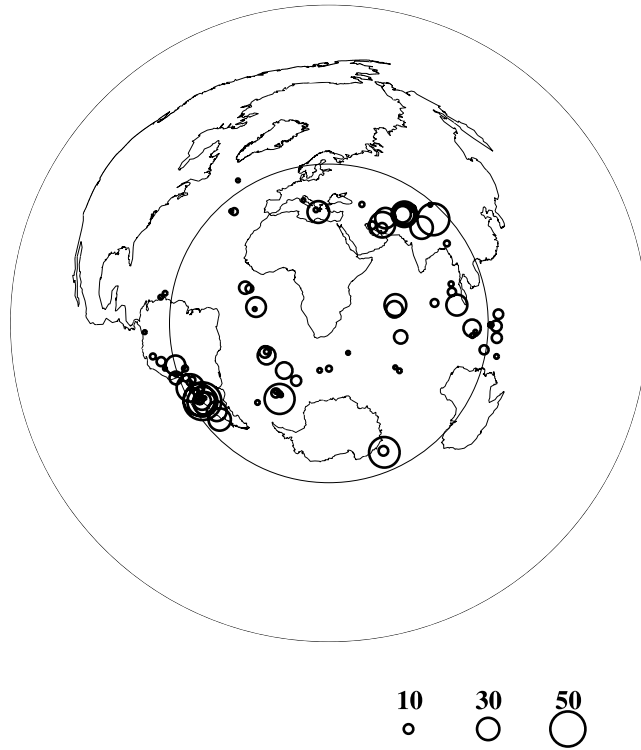
Figure 2. Locations of the events used in the study. The size of the circles is proportional to the number of high-quality receiver functions from the event.

the time domain. The positive *PṁS* and *PPṁS* and the negative *PSṁS* phases can be observed clearly. Examples of original receiver functions can be found in Figure 4. A reliable determination of ϕ depends on clear *PPṁS* and *PSṁS* arrivals, which are found at more than half of the stations. A few stations, most of which were located at the southern portion of the study area, recorded a limited number of high-quality seismograms and consequently reliable results were not obtained in some of these cases.

3. Methods

3.1. Searching for the Optimal H and ϕ

[18] Most of the previous measurements of H and ϕ have come from one of the following two groups of techniques. The first group uses active source seismic refraction (and reflection) experiments in which both *P* and *S* waves are generated [*Holbrook et al.*, 1992; *Egorkin*, 1998]. The major difficulty of active source seismic experiments is that they involve a large number of seismographs, and are labor intensive and expensive [*Chevrot and van der Hilst*, 2000], especially when *S* waves are generated and recorded at a high signal/noise ratio.

[19] Another group of techniques utilizes the travel times of *P*−to−*S* converted waves from the Moho and the multiple reverberations generated from teleseismic body waves [*Clarke and Silver*, 1993; *Zandt et al.*, 1995; *Zandt and Ammon*, 1995; *Chevrot and van der Hilst*, 2000; *Zhu and Kanamori*, 2000]. In this study we stack radial receiver functions from many events along the travel time curves of the converted and reflected phases at the Moho to find the

crustal thickness and V_p/V_s (H and ϕ) that give rise to the maximum stacking amplitude [*Chevrot and van der Hilst*, 2000; *Zhu and Kanamori*, 2000]. We apply a series of candidate depths H_i in the range from 30 to 65 km in increments of 0.1 km, and candidate ϕ_j from 1.65 to 1.85 in increments of 0.0025.

[20] For each pair of (H_i, ϕ_j), we calculate the moveout of *PṁS*, $t_1^{(i,j)}$, using [*Sheriff and Geldart*, 1993; *Dueker and Sheehan*, 1998]

$$t_1^{(i,j)} = \int_{-H_i}^{0} \left[\sqrt{\left(V_p(z)/\phi_j\right)^{-2} - p^2} - \sqrt{V_p(z)^{-2} - p^2} \right] dz \quad (1)$$
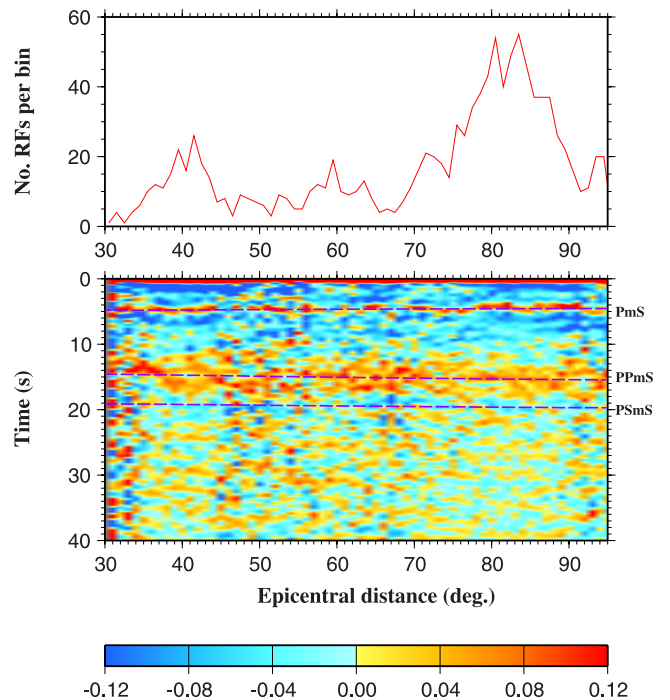
where p is the *P* wave ray parameter, H_i is the depth of the candidate discontinuity, ϕ_j is the candidate V_p/V_s, and $V_p(z)$ is the *P* wave velocity at depth z.

[21] The moveout, $t_2^{(i,j)}$ of *PPṁS* can be calculated using

$$t_2^{(i,j)} = \int_{-H_i}^{0} \left[\sqrt{\left(V_p(z)/\phi_j\right)^{-2} - p^2} + \sqrt{V_p(z)^{-2} - p^2} \right] dz \quad (2)$$

and that of *PSṁS*, $t_3^{(i,j)}$, is

$$t_3^{(i,j)} = \int_{-H_i}^{0} 2\sqrt{\left(V_p(z)/\phi_j\right)^{-2} - p^2} \, dz \quad (3)$$

Figure 3. (bottom) Binned and stacked 1544 radial receiver functions used in the study. Dashed lines are predicted moveout curves for *PṁS*, *PPṁS*, and *PSṁS* calculated on the basis of the IASP91 Earth model [*Kennett and Engdahl*, 1991] with a Moho at 35 km depth. Amplitudes are normalized to *P* wave amplitudes on radial receiver functions. (top) Number of receiver functions per bin.
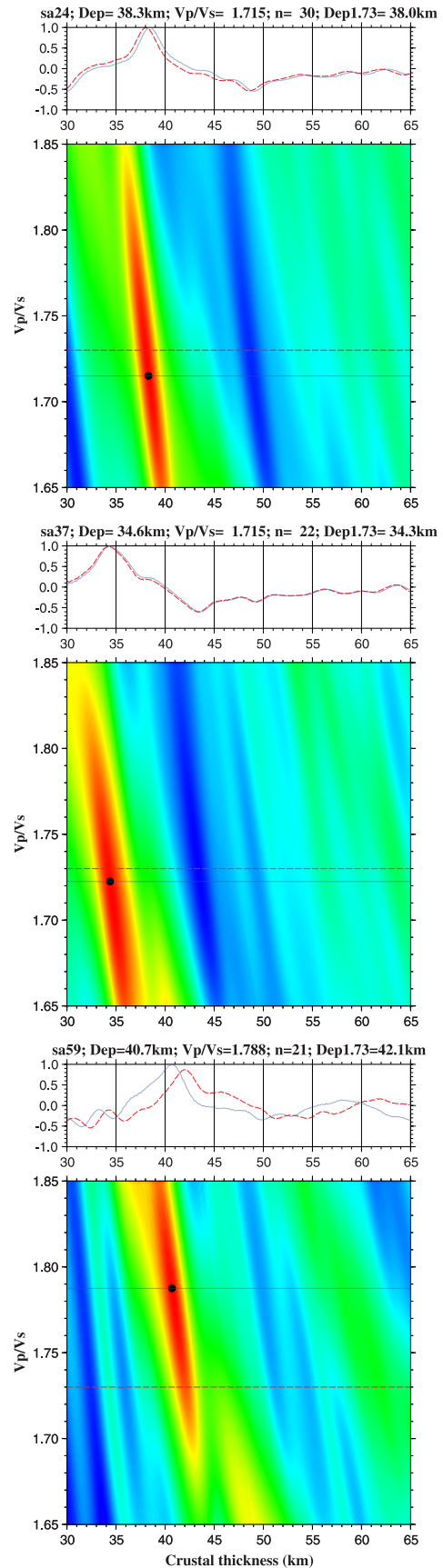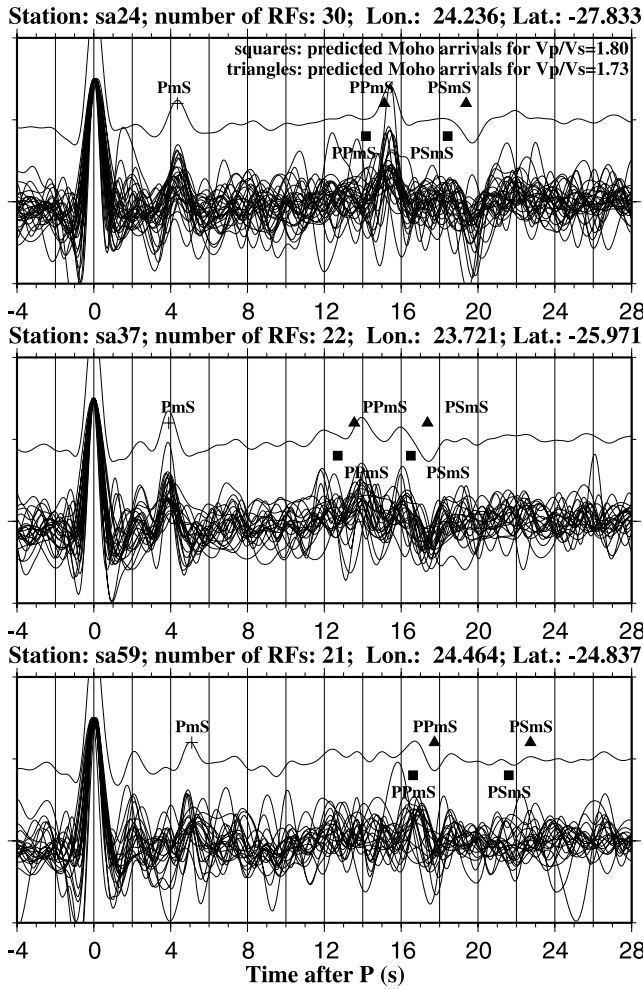
Figure 4. Example receiver functions from three stations. For each station, the single trace at the top of the individual receiver functions is the result of simple time domain summation (without moveout correction) of the individual traces. Triangles are theoretical arrival times for $PP\breve{m}S$ and $PS\breve{m}S$ calculated using equations (2) and (3) by taking $p = 5.0$ s/deg, $V_p = 6.5$ km/s, and $\phi = 1.73$. H in the equations is calculated based on the observed arrival times of $P\acute{m}S$. Squares are theoretical arrival times calculated using $\phi = 1.80$. The rightward shift of the observed reverberations relative to the triangles for sa24 and sa37 suggests that the actual ϕ is smaller than 1.73. For sa59, the similarity between the observed and predicted arrival times for $\phi = 1.80$ (squares) suggests that the actual ϕ is close to 1.80.

Figure 5. H-ϕ plots for the three stations shown in Figure 4. For each station, the dashed line in the top plot shows stacking amplitudes for $\phi = 1.73$; that is, it is a cross section along the dashed line in the bottom plot. The solid line was produced using the optimal ϕ. The resulting crustal thickness, ϕ, and the crustal thickness when $\phi = 1.73$ is assumed (denoted as Dep1.73) are shown on the top panels. Those results are consistent with direct observations made on the original receiver functions shown in Figure 4.
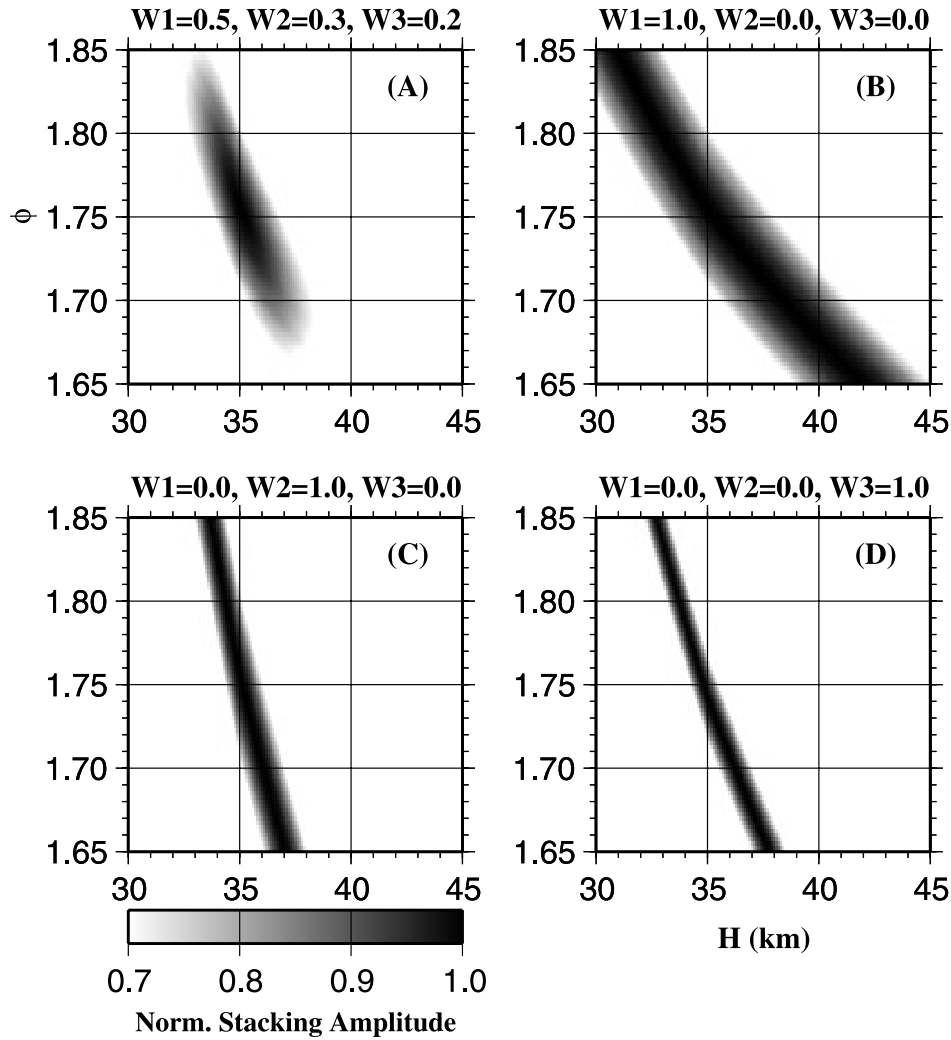
Figure 6. H-ϕ plots for four combinations of the weighting factors. The plots were created using 66 CORE synthetic seismograms based on equations (1)–(4). Darker regions have higher stacking amplitude. Only regions with normalized stacking amplitude $\geq 70\%$ ($0.7 - 1.0$) of the maximum stacking amplitude are plotted.

[22] The receiver functions at each of the stations are then stacked using

$$A(H_i, \phi_j) = \sum_{k=1}^{n} w_1 S_k\left(t_1^{(i,j)}\right) + w_2 S_k\left(t_2^{(i,j)}\right) - w_3 S_k\left(t_3^{(i,j)}\right) \quad (4)$$

where n is the number of radial receiver functions from the station, $S_k(t)$ is the amplitude of the point on the kth receiver function at time t after the first P arrival (where $t = t_1$, t_2 or t_3), and w_1, w_2, and w_3 are weighting factors that satisfy $w_1 + w_2 + w_3 = 1$ [*Zhu and Kanamori*, 2000]. The optimal pair of (H_i, ϕ_j) is the one that gives the maximum stacking amplitude.

[23] On the basis of the observation that the S/N of *PṁS* is the largest and that of *PSṁS* is the smallest (Figure 3), in this study we use 0.5, 0.3, and 0.2 for the weighting factors, respectively. Relative to the values used by *Zhu and Kanamori* [2000] (0.7, 0.2, and 0.1) and *Chevrot and van*

der Hilst [2000] (0.5, 0.5, and 0.0), we used a larger weighting factor for *PSṁS* because of its strong appearance on the original receiver functions (Figure 4). Examples of (H, ϕ) plots can be found in Figure 5.

3.2. Synthetic Test

[24] We test the above procedure using Complete Ordered Ray Expansion (CORE [*Clarke and Silver*, 1991]) synthetic seismograms. We generate 66 seismograms for the epicentral distance range from 30° to 95° with a "station" interval of 1° using a velocity model with a Moho at 35 km depth, a crustal V_p of 6.5 km/s, and a crustal ϕ of 1.75, convert them into radial receiver functions, and stack them based on equations (1)–(4).

[25] When only *PṁS* is used, there is a nearly complete tradeoff between H_i and ϕ_j (Figure 6b), as expected. Such a tradeoff is also apparent when *PPṁS* (Figure 6c) or *PSṁS* is used alone (Figure 6d). The tradeoff can be significantly reduced if two or three phases are used simultaneously, because their (H, ϕ) curves have different slopes (Figure 6a).
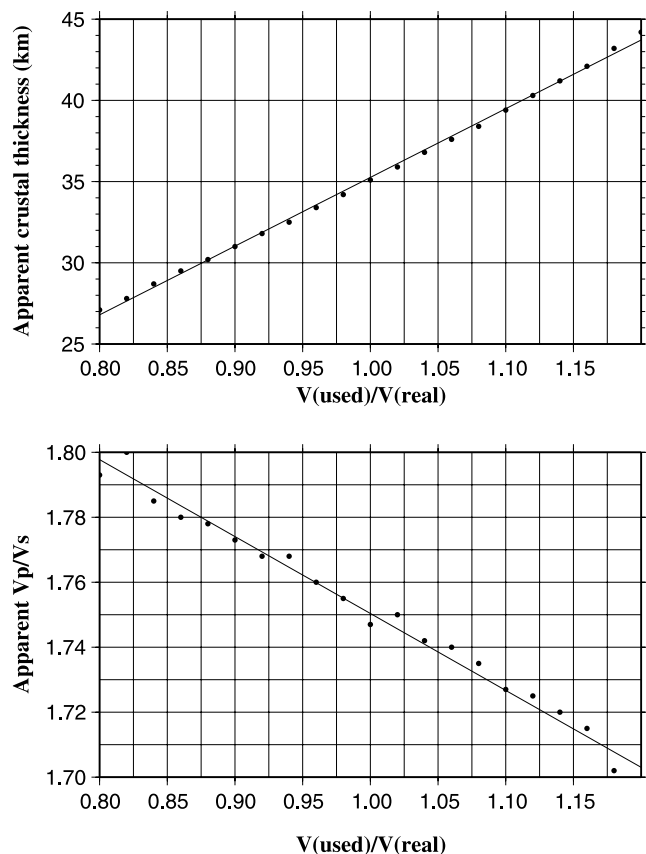
Figure 7. Variations of (top) the resulting apparent crustal thickness and (bottom) ϕ as a function of velocity bias, based on stacking of 66 CORE synthetic seismograms.

3.3. Error Estimate

[26] *Zhu and Kanamori* [2000] used a Taylor expansion to measure the flatness of $A(H_i, \phi_j)$ in the vicinity of the optimal pair of parameters to get the standard deviation (STD) of H and ϕ. Our tests indicate that STDs estimated using the Taylor expansion approach are dependent on the number of data points used to calculate the derivatives. They are also functions of filtering parameters, and are thus unstable. In this study we use the bootstrap method [*Press et al.*, 1992; *Efron and Tibshirani*, 1986] to estimate the standard deviations of the optimal H and ϕ. For each bootstrap step, we randomly choose $1 - 1/e = 63\%$ independent receiver functions that belong to a station. About 60% of the chosen ones are then duplicated so that the total number of the new set of receiver functions is the same as that of the original set. Equations (1)–(4) are used on the new set of receiver functions to produce images of discontinuities. The resulting H and ϕ for the station are expected to be normally distributed around the true values [*Press et al.*, 1992].

### 3.4. Effects of Uncertainties in Crustal Velocity

[27] In order to obtain estimates of H and ϕ it is necessary to specify a reference crustal velocity, $V_p(z)$. Consequently, errors in $V_p(z)$ will map into errors in these parameters. The value we have chosen for $V_p(z)$ is 6.5 km/s, and is based on a previous seismic refraction study [*Durrheim and Green*, 1992].

[28] We estimate this source of uncertainty by stacking the 66 CORE synthetic seismograms. As shown in Figure 7, both the resulting H and ϕ display a linear dependence on the ratio between crustal velocity used for the stacking and that used to generate the synthetics. The best fitting slopes are 0.46 km per 1% of velocity bias for H, and -0.0024 per 1% bias in velocity for ϕ. In southern Africa, sparse seismic refraction profiles revealed a small spatial variation in mean crustal velocity, probably less than 5% [*Durrheim and Green*, 1992]. This corresponds to an uncertainty of less than 3 km in the resulting H. Similarly, errors of several percent in velocity model has insignificant effect on the resulting ϕ. This is consistent with the conclusions from previous studies [*Clarke and Silver*, 1993; *Zhu and Kanamori*, 2000]. Indeed, the expected error in ϕ is roughly an order of magnitude smaller than the range that we observe in the data.

3.5. Quantification of the Sharpness of the Moho

[29] The sharpness of the Moho is related to the thickness of the transition zone from the crust to the mantle. A sharp Moho produces strong *PmS* and its multiples. There are several other factors that can affect the amplitude of the converted phases. The first is the lateral variation in Moho depth. While significant short-wavelength variations cannot be ruled out, our resulting crustal thickness (see Figure 8) suggests that the Moho in the study area is fairly flat, and thus variation in Moho depth is unlikely to significantly affect the amplitude of the converted phases. The second is velocity heterogeneities in the crust beneath the area surrounding a station. The crustal volume traversed by the rays is approximately cone shaped, with a maximum radius of about 10 km (for an event 30° away). Difference in velocities within the volume results in incoherent stacking and consequently reduction in the stacked amplitude of the converted phases. For instance, based on equations (1)–(3), for a Moho depth of 35 km and a P wave ray parameter $p = 5.725$ s/deg (epicentral distance $\Delta = 75.5°$), a lateral velocity variation of 3% leads to a change of 0.12 s in t_1, 0.47 s in t_2, and 0.59 s in t_3. These arrival time differences are several times smaller than the width of the phases used (e.g., Figure 4), and thus would not likely affect the stacking amplitude significantly. The third influence is the contrasts of the P and S wave velocities across the Moho. The resulting sixfold spatial variation in the amplitudes (see Figure 9), however, has ruled out the possibility that this parameter plays the dominant role in the observed variation of the amplitudes of the converted phases. The other influence is the topography of velocity interfaces in the crust. The simplicity of most of the receiver functions (e.g., Figure 4), however, suggests that the interfaces, if they exist, are weak and thus should not significantly affect the amplitudes of the converted phases.

[30] By stacking *PmS* receiver functions using a constant ϕ of 1.73 for all the stations, *Nguuri et al.* [2001] found that the stacked amplitude of *PmS* in areas with thick crust, such as the Bushveld Complex and most of the Limpopo belt, is smaller than that in areas with thin crust. They proposed that the Moho beneath the former areas was disturbed by Proterozoic events and is thus less sharp. For the Bushveld Complex, another possible cause of the observed small stacking amplitudes is that the *PmS* phases
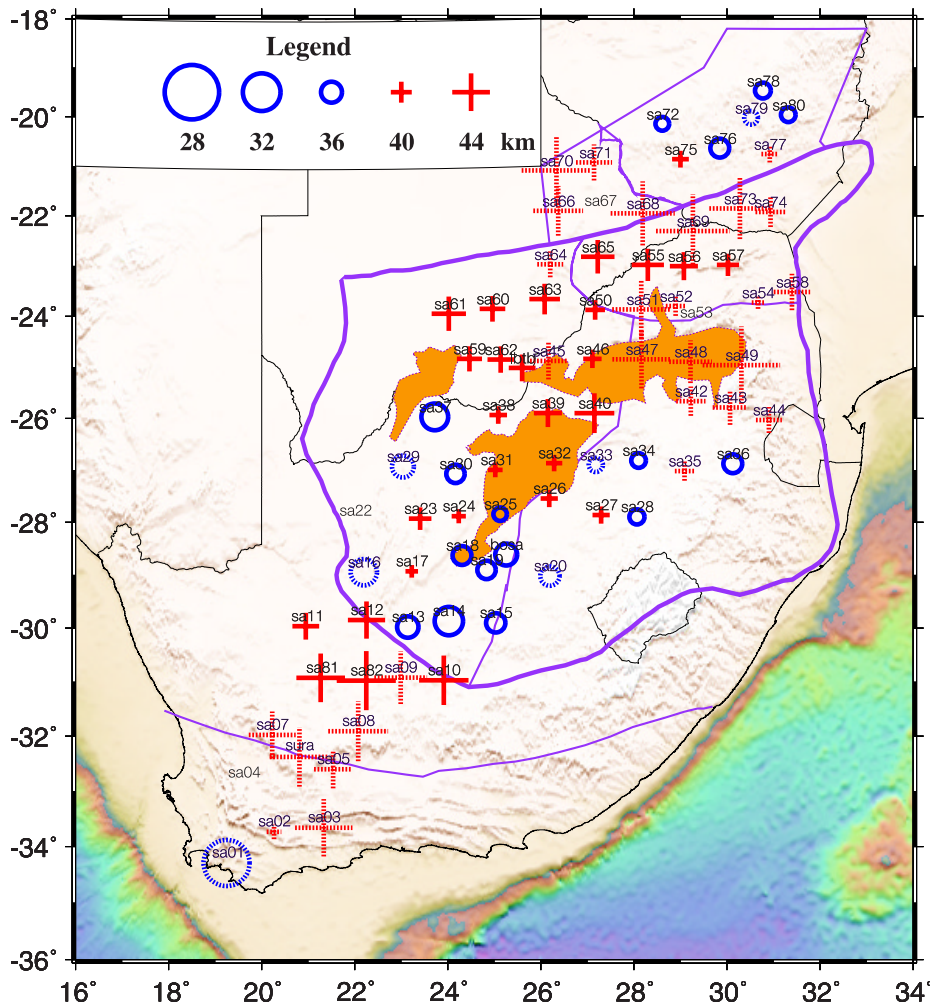
Figure 8. Resulting crustal thickness (H). Open circles represent stations with a smaller thickness, and pluses are stations with a larger thickness (see legend). Solid symbols are category A stations, and dotted ones are category B stations.

originated from a deeper Moho are stacked less coherently, because the φ values in this area are significantly larger than 1.73, which was the value used for the stacking by *Nguuri et al.* [2001].

[31] To quantify the apparent sharpness of the Moho beneath a station, we measure R, the ratio between the stacking amplitude corresponding to the optimal pair of (H, φ) and the mean amplitude of the direct P wave on the radial components. Although R is a function of the angle of incidence, the fact that most of the events have an epicentral distance that is $\geq 70°$ (Figure 3) suggests that most of the rays arrive at the station at a near-vertical angle, and thus are weakly affected by variations in the incident angle. In addition, the resulting distribution of R shows a high level of spatial consistency (see Figure 9) and correspondence with geologic provinces (Figure 1), suggesting that the resulting R values indeed reflect the sharpness of the Moho.

4. Results

[32] Observations of H, R, and φ were obtained at most of the 82 stations (Figures 8–10 and Table 1). On the basis of the quality of the original receiver functions, we divide the results into three categories. Those in category A (44 in total) display a clear arrival in the time window of 3.5–6 s, which is considered as PmS, and at least one of the multiples near the vicinity of the predicted arrival times (calculated using φ = 1.73; see Figure 4 for examples). For most of the category A stations, a well-defined peak on the H-φ plot is consistently observed, and therefore both H and φ can be determined with high confidence.

[33] Category B stations show clear PmS but not $PPmS$ or $PSmS$ arrivals. Thus an optimal pair of (H, φ) cannot be unambiguously determined. For those stations we can still obtain an estimate of the crustal thickness by assuming a "nominal" φ of 1.73. Obviously, a larger departure of the real φ beneath a station from 1.73 results in greater error in the estimated thickness (H_n). The magnitude of the error, however, is about 2 km or less if we assume that the actual φ values under those category B stations are within the range of the φ values obtained at the category A stations (Figure 11). The other option is to use the φ value found for nearby stations, since the φ distribution is fairly smooth. However, this would make an insignificant difference compared to the approach above, given the weak dependence of H on φ (Figure 11). A total of 34 stations belong to
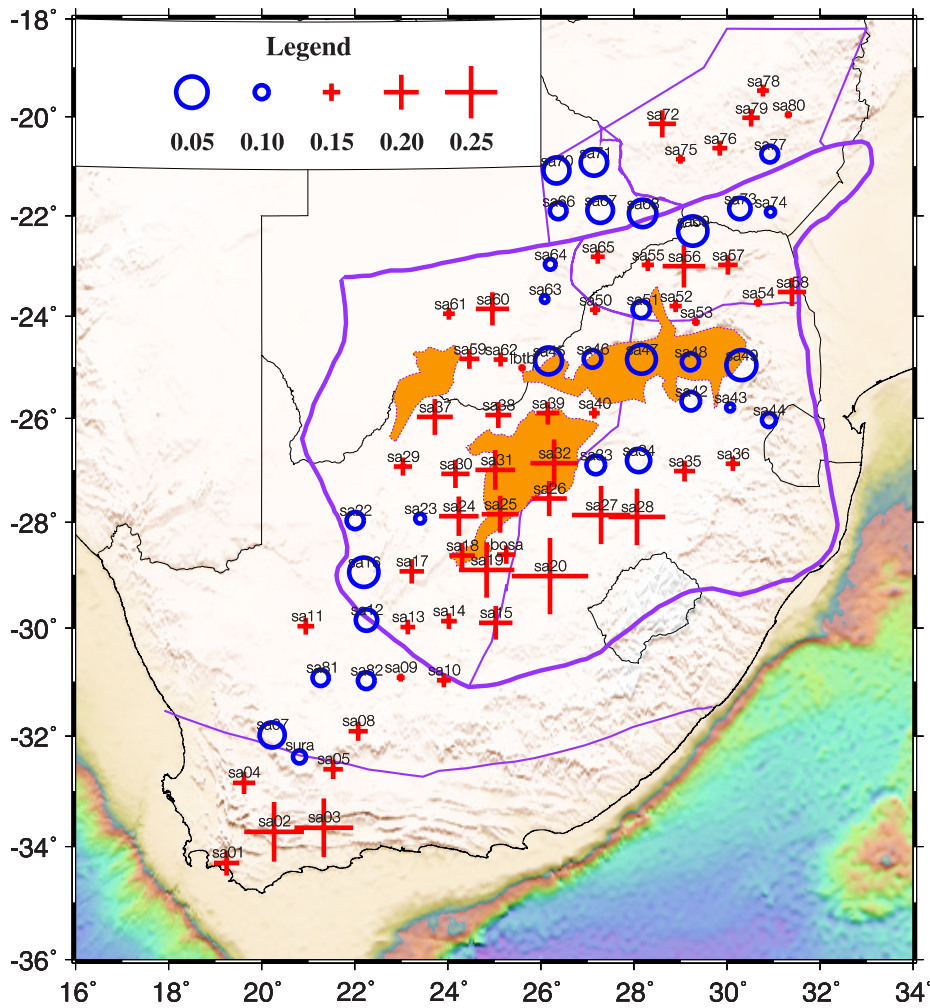
Figure 9. Resulting ratio (R) of the stacking amplitude corresponding to the optimal pair of (H, φ) over that of direct P wave on the radial component. R calculated for all stations.

this category. In the following discussion, H is used for category A stations, and H_n is used for category B stations.

[34] None of the three Moho phases used in the study can be clearly observed at the four stations in category C, and therefore neither H nor φ can be determined. For those stations, the resulting maximum stacking amplitude (R) is small and mostly reflects the noise level.

[35] For the entire study area, the resulting φ values range from 1.70 to 1.82, with a mean of 1.74, and the crustal thickness ranges from 30 to 54 km, with a mean of 41 km. The R values have a mean of 0.14 with a range of 0.05−0.32, a sixfold difference. As indicated in Table 1, the magnitude of the spatial variations of the parameters is significantly larger than the STD of most of the individual measurements, suggesting that the variations are well constrained.

[36] In the following, we divide the study area into six subareas based on the characteristics of the measurements, tectonic history, and surface geology. The mean values of the resulting parameters for each of the areas can be found in Table 2.

4.1. Eastern Zimbabwe Craton (Area A)

[37] The crustal thickness beneath the eastern Zimbabwe craton is among the smallest (38 km), but the φ (1.73) and R

(0.135) measurements are close to the average value for the entire study area. Both H and φ are spatially consistent, as indicated by the small STD (Table 2).

4.2. Western Zimbabwe Craton (Area B)

[38] $P\acute{m}S$ phases are weak at all of the five stations, and none of the stations shows observable $PP\check{m}S$ or $PS\check{m}S$. The averaged H over the five stations in this area (48 km) is the largest, and the R values (0.070) are the smallest in the entire study area. Although traditionally areas A and B are considered as a single tectonic unit (the Zimbabwe craton), the large contrast in crustal thickness and sharpness between the two areas suggests that the crust has different characteristics.

4.3. The Limpopo Belt and Adjacent Areas (Area C)

[39] The Limpopo belt is characterized by a thick crust (~44 km) and comparable φ values (1.74) with those observed on the eastern Zimbabwe and southern Kaapvaal cratons (see below). The R values observed in the central part of the area are higher than those observed on the northern and southern edges, and the crustal thickness shows an increasing trend toward the edges (Figure 8). The thick crust and relatively low R values of the adjacent
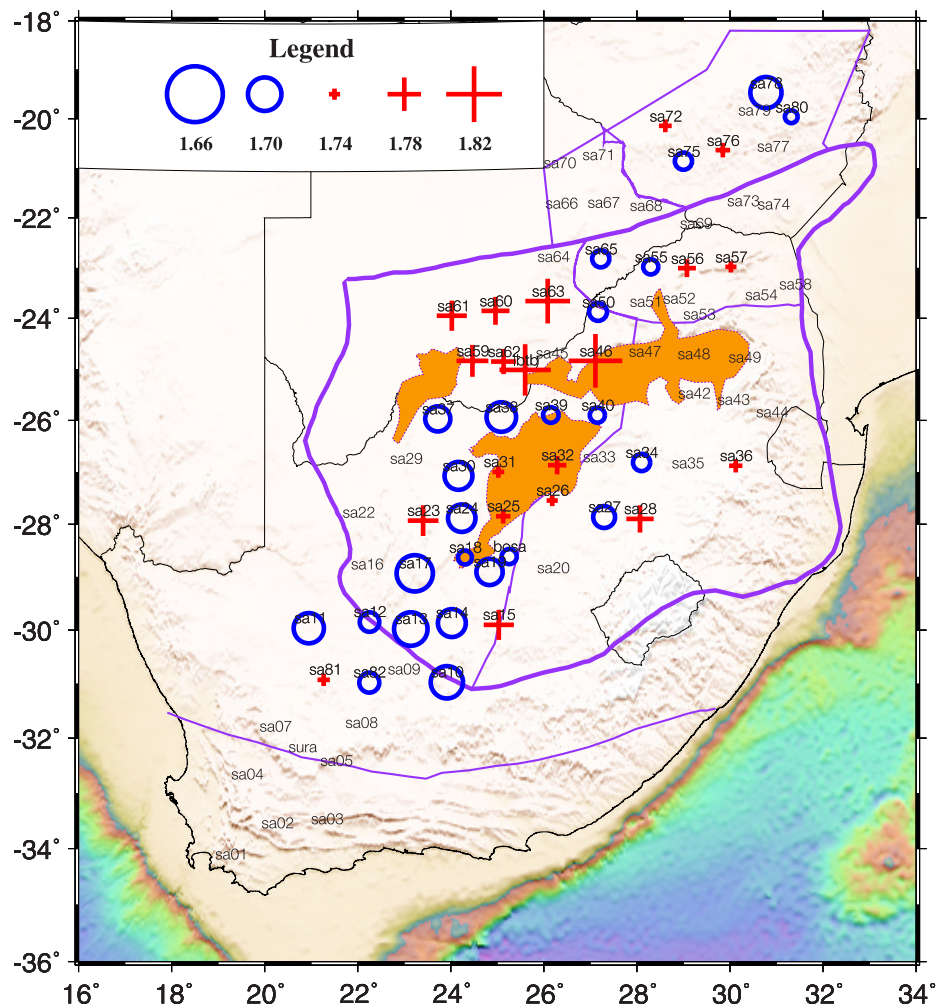
Figure 10. Resulting crustal V_p/V_s (ϕ) for category A stations.

western Zimbabwe craton are similar to those found for the Limpopo belt, suggesting that the Limpopo deformation may in fact extend into that region. Indeed, such a westward extension of the Limpopo has been proposed, based on the Limpopo-related gravity anomaly that underlies this zone [*Ranganai et al.*, 2002].

4.4. The Bushveld Complex and Vicinity (Area D)

[40] Some of the largest ϕ values and thickest crust in the study area are found beneath the Bushveld Mafic Intrusion Complex and its surrounding areas. This area is also characterized by very small R values. The region with large ϕ, large H, and small R measurements actually covers an area that includes but is much larger than the surface expression of the Complex. If this is related to the Bushveld, it suggests that its lateral extent in the crust is much greater than what is exposed at the surface. Examination of potential field data also provides evidence for a larger area at depth [*Webb et al.*, 2004].

4.5. Southern Kaapvaal Craton (Area E)

[41] Similar to the eastern Zimbabwe craton, the southern part of the Kaapvaal craton (approximately south of 26°S) shows some of the thinnest crust, smallest ϕ, and largest R values in the study area. The R values are the largest in the

central part of this area, and decrease gradually toward the western and southern edges (Figure 9). Beneath the Kimberly array, which is between stations sa18 and bosa, *Niu and James* [2002] found an average ϕ of 1.73 and a crustal thickness of 35.4 km. Those are essentially the same as our results obtained at sa18 (1.74 and 36.5 km), and those at bosa (1.73 and 35.8 km). While the results of H obtained by *Stankiewicz et al.* [2002] are statistically consistent with those from the present study, most of their ϕ observations are significantly larger (1.74 ± 0.02, 1.78 ± 0.02, and 1.78 ± 0.02 for the three earthquakes) as noted previously. At sa23, which is located near the eastern boundary of the Kheis belt, a high ϕ (1.78) is observed. Similar to those within the Bushveld Complex but with smaller contrast, stations inside the Ventersdorp zone of Neoarchean rifting and magmatism, sa25, sa26, sa31, and sa32, show larger ϕ and larger H relative to the surrounding regions.

4.6. Post-Archean Fold Belts (Area F)

[42] The crust beneath the Proterozoic (1.1–1.9 Ga) Namaqua-Natal mobile belt is among the thickest in the study area. While the contrast in H between this area and the southern Kaapvaal craton is sudden and significant (about 6 km), the ϕ values obtained at the two areas are similar.

Table 1. Observations of Crustal Thickness (H, H_n), V_p/V_s (ϕ), and R

Station	Region	Longitude, deg,	Latitude deg,	H, km	ϕ	H_n, km	R	N^a	Rank
bosa	E	25.256	−28.614	35.8 ± 0.15	1.733 ± 0.007	35.8 ± 0.04	0.153 ± 0.018	29	A
lbtb	D	25.597	−25.015	41.4 ± 0.49	1.812 ± 0.020	43.5 ± 0.22	0.121 ± 0.067	31	A
sa01	F	19.246	−34.294	–	–	30.0 ± 0.18	0.172 ± 0.022	5	B
sa02	F	20.266	−33.735	–	–	38.5 ± 1.03	0.271 ± 0.070	3	B
sa03	F	21.335	−33.662	–	–	48.7 ± 0.00	0.268 ± NaN	1	B
sa04	F	19.621	−32.851	–	–	–	0.164 ± 0.054	6	C
sa05	F	21.535	−32.605	–	–	44.1 ± 1.48	0.156 ± 0.046	4	B
sa07	F	20.226	−31.978	–	–	46.2 ± 0.81	0.068 ± 0.013	24	B
sa08	F	22.073	−31.910	–	–	49.3 ± 0.31	0.155 ± 0.050	6	B
sa09	F	22.986	−30.922	–	–	47.6 ± 0.46	0.123 ± 0.024	5	B
sa10	F	23.914	−30.972	46.8 ± 0.89	1.702 ± 0.022	46.0 ± 0.45	0.140 ± 0.021	5	A
sa11	F	20.947	−29.965	41.4 ± 0.15	1.706 ± 0.004	40.8 ± 0.16	0.148 ± 0.020	11	A
sa12	F	22.253	−29.849	43.9 ± 0.27	1.725 ± 0.010	43.7 ± 0.12	0.079 ± 0.008	23	A
sa13	E	23.140	−29.979	35.9 ± 0.65	1.700 ± 0.014	35.3 ± 0.30	0.142 ± 0.026	12	A
sa14	E	24.023	−29.868	34.2 ± 0.25	1.710 ± 0.013	33.7 ± 0.05	0.145 ± 0.034	12	A
sa15	E	25.031	−29.902	36.4 ± 0.34	1.774 ± 0.016	37.3 ± 0.09	0.196 ± 0.023	7	A
sa16	E	22.195	−28.950	–	–	34.7 ± 0.19	0.056 ± 0.017	19	B
sa17	E	23.226	−28.932	38.0 ± 0.39	1.695 ± 0.011	37.1 ± 0.20	0.170 ± 0.016	27	A
sa18	E	24.306	−28.633	36.5 ± 0.94	1.735 ± 0.018	36.6 ± 0.49	0.173 ± 0.012	19	A
sa19	E	24.833	−28.906	36.6 ± 0.51	1.713 ± 0.014	36.2 ± 0.21	0.259 ± 0.012	8	A
sa20	E	26.195	−29.022	–	–	36.4 ± 0.87	0.319 ± 0.020	8	B
sa22	E	22.009	−27.966	–	–	–	0.091 ± 0.020	10	C
sa23	E	23.405	−27.930	40.4 ± 0.28	1.775 ± 0.008	41.3 ± 0.27	0.112 ± 0.007	27	A
sa24	E	24.236	−27.883	38.4 ± 0.23	1.711 ± 0.011	38.0 ± 0.03	0.213 ± 0.021	30	A
sa25	E	25.126	−27.846	37.8 ± 0.34	1.746 ± 0.009	38.3 ± 0.10	0.206 ± 0.010	27	A
sa26	E	26.180	−27.545	39.1 ± 0.27	1.740 ± 0.009	39.4 ± 0.14	0.201 ± 0.023	5	A
sa27	E	27.294	−27.862	39.1 ± 0.23	1.721 ± 0.008	38.9 ± 0.10	0.267 ± 0.030	7	A
sa28	E	28.066	−27.898	37.4 ± 0.42	1.769 ± 0.025	38.3 ± 0.18	0.262 ± 0.012	3	A
sa29	E	23.035	−26.932	–	–	35.8 ± 0.08	0.152 ± 0.020	13	B
sa30	E	24.165	−27.072	36.6 ± 0.35	1.710 ± 0.012	36.2 ± 0.15	0.181 ± 0.024	9	A
sa31	E	25.021	−26.995	38.5 ± 0.21	1.741 ± 0.008	38.8 ± 0.00	0.214 ± 0.009	20	A
sa32	E	26.285	−26.865	38.9 ± 0.21	1.753 ± 0.008	39.4 ± 0.08	0.236 ± 0.027	22	A
sa33	E	27.179	−26.899	–	–	37.6 ± 1.36	0.087 ± 0.026	5	B
sa34	E	28.099	−26.814	37.5 ± 0.21	1.729 ± 0.003	37.5 ± 0.29	0.073 ± 0.006	10	A
sa35	E	29.088	−27.018	–	–	39.6 ± 0.55	0.160 ± 0.057	4	B
sa36	E	30.125	−26.877	36.5 ± 0.38	1.744 ± 0.013	36.7 ± 0.25	0.141 ± 0.018	13	A
sa37	E	23.721	−25.971	34.6 ± 0.24	1.715 ± 0.010	34.3 ± 0.10	0.203 ± 0.008	22	A
sa38	E	25.085	−25.933	39.2 ± 0.23	1.707 ± 0.009	38.6 ± 0.06	0.174 ± 0.016	29	A
sa39	E	26.151	−25.895	41.7 ± 0.36	1.732 ± 0.009	41.7 ± 0.25	0.166 ± 0.008	21	A
sa40	D	27.149	−25.898	44.5 ± 2.36	1.733 ± 0.042	44.8 ± 0.58	0.131 ± 0.010	32	A
sa42	D	29.222	−25.665	–	–	42.0 ± 0.84	0.087 ± 0.016	8	B
sa43	D	30.067	−25.787	–	–	43.3 ± 0.25	0.117 ± 0.010	4	B
sa44	D	30.902	−26.032	–	–	41.2 ± 1.88	0.100 ± 0.017	9	B
sa45	D	26.164	−24.879	–	–	43.8 ± 0.21	0.063 ± 0.006	36	B
sa46	D	27.109	−24.838	39.4 ± 0.42	1.816 ± 0.018	42.3 ± 2.05	0.089 ± 0.015	34	A
sa47	D	28.162	−24.847	–	–	48.9 ± 1.34	0.057 ± 0.010	25	B
sa48	D	29.216	−24.895	–	–	45.2 ± 0.17	0.091 ± 0.017	10	B
sa49	D	30.309	−24.960	–	–	53.5 ± 0.32	0.054 ± 0.016	9	B
sa50	D	27.166	−23.872	39.7 ± 0.22	1.728 ± 0.007	39.6 ± 0.28	0.129 ± 0.016	19	A
sa51	D	28.157	−23.863	–	–	48.9 ± 0.94	0.090 ± 0.012	27	B
sa52	D	28.897	−23.798	–	–	39.7 ± 0.91	0.135 ± 0.037	3	B
sa53	D	29.333	−24.113	–	–	–	0.122 ± 0.028	4	C
sa54	C	30.668	−23.729	–	–	38.0 ± 2.65	0.124 ± 0.014	7	B
sa55	C	28.298	−22.980	42.7 ± 0.39	1.733 ± 0.007	42.8 ± 0.16	0.135 ± 0.011	38	A
sa56	C	29.074	−23.006	41.7 ± 0.22	1.752 ± 0.008	42.3 ± 0.09	0.222 ± 0.015	36	A
sa57	C	30.020	−22.981	40.3 ± 0.31	1.740 ± 0.012	40.6 ± 0.11	0.156 ± 0.009	32	A
sa58	C	31.397	−23.518	–	–	43.7 ± 0.85	0.181 ± 0.049	3	B
sa59	D	24.464	−24.837	41.0 ± 0.19	1.777 ± 0.008	42.1 ± 0.13	0.157 ± 0.016	21	A
sa60	D	24.959	−23.852	41.1 ± 0.14	1.770 ± 0.004	42.3 ± 0.33	0.195 ± 0.026	17	A
sa61	D	24.022	−23.948	43.2 ± 0.35	1.774 ± 0.013	44.7 ± 0.86	0.134 ± 0.011	17	A
sa62	D	25.135	−24.851	41.3 ± 0.55	1.765 ± 0.012	42.3 ± 0.27	0.140 ± 0.011	19	A
sa63	D	26.082	−23.658	42.3 ± 0.26	1.800 ± 0.010	44.4 ± 1.12	0.119 ± 0.012	21	A
sa64	C	26.202	−22.969	–	–	41.2 ± 0.58	0.109 ± 0.014	17	B
sa65	C	27.222	−22.818	43.0 ± 0.17	1.729 ± 0.005	43.1 ± 0.07	0.140 ± 0.011	22	A
sa66	B	26.373	−21.900	–	–	46.9 ± 0.16	0.092 ± 0.018	22	B
sa67	B	27.274	−21.886	–	–	–	0.067 ± 0.014	21	C
sa68	B	28.188	−21.950	–	–	50.3 ± 1.19	0.061 ± 0.010	19	B
sa69	C	29.266	−22.305	–	–	52.6 ± 4.55	0.056 ± 0.012	17	B
sa70	B	26.335	−21.088	–	–	51.6 ± 0.23	0.065 ± 0.011	24	B
sa71	B	27.141	−20.926	–	–	43.6 ± 0.85	0.064 ± 0.013	15	B
sa72	A	28.611	−20.143	37.7 ± 0.15	1.743 ± 0.006	38.0 ± 0.07	0.178 ± 0.012	33	A
sa73	C	30.278	−21.854	–	–	49.6 ± 0.39	0.079 ± 0.037	23	B
sa74	C	30.936	−21.923	–	–	42.2 ± 0.15	0.114 ± 0.012	25	B

Table 1. (continued)

Station	Region	Longitude, deg,	Latitude deg,	H, km	ϕ	H_n, km	R	N^a	Rank
sa75	A	28.999	−20.860	39.0 ± 0.23	1.729 ± 0.008	39.1 ± 0.07	0.126 ± 0.005	34	A
sa76	A	29.846	−20.636	36.5 ± 0.21	1.746 ± 0.007	36.9 ± 0.14	0.143 ± 0.009	44	A
sa77	A	30.919	−20.756	−	−	39.0 ± 0.94	0.092 ± 0.015	30	B
sa78	A	30.772	−19.467	37.2 ± 0.34	1.704 ± 0.013	36.6 ± 0.16	0.134 ± 0.007	34	A
sa79	A	30.517	−20.021	−	−	37.7 ± 0.13	0.150 ± 0.022	11	B
sa80	A	31.318	−19.959	37.5 ± 0.26	1.737 ± 0.013	37.7 ± 0.13	0.121 ± 0.022	23	A
sa81	F	21.268	−30.925	46.6 ± 1.19	1.742 ± 0.031	46.9 ± 0.40	0.093 ± 0.009	19	A
sa82	F	22.247	−30.977	49.1 ± 0.46	1.724 ± 0.012	49.0 ± 0.23	0.092 ± 0.025	24	A
sura	F	20.812	−32.380	−	−	49.2 ± 1.76	0.103 ± 0.017	15	B

[a]N is the number of receiver functions used.
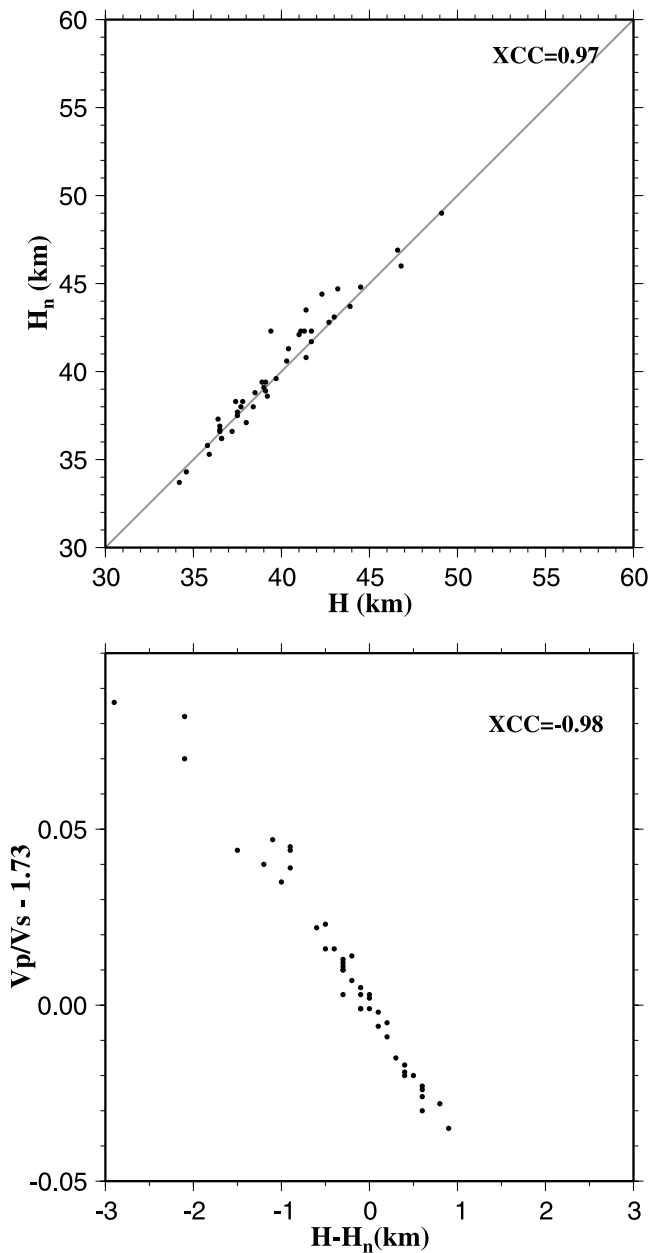
Figure 11. (top) Comparison of crustal thicknesses obtained using variable ϕ values with those using a ϕ fixed at 1.73 for category A stations. XCC stands for cross-correlation coefficient. (bottom) Relationship between variations of ϕ and those of H.

[43] Reliable ϕ measurements could not be determined at any of the stations on the Paleozoic Cape Fold Belt, which was stabilized at about 0.3 Ga. In the southern half of this area, the crustal thickness shows a southward thinning, from about 49 km to about 30 km.

5. Discussion

5.1. Comparison of H With Previous Measurements

[44] Our estimates of H are broadly consistent with the results of previous studies. *Nguuri et al.* [2001] stacked about 1300 *PḿS* arrivals from 35 teleseismic events, using the procedure of *Dueker and Sheehan* [1998] and obtained measurements of crustal thickness at the same stations used in our study. They also found relatively thin crust in the southern Kaapvaal and Zimbabwe cratons, and relatively thick crust beneath the Bushveld, and the collision zones of the Limpopo and Namaqua-Natal regions. There are some discrepancies, however, due to a difference in analysis methods. *Nguuri et al.* [2001] made their measurements under the assumption of a constant ϕ of 1.73, a constant crustal velocity of 6.5 km/s, and a reference Moho depth of 38 km. Below this depth, the mantle P wave velocity of the IASP91 Earth model was used. Figure 12 shows the comparisons of their results with our measurements of H_n and H.

[45] While the agreement between the two sets of results is generally good, for stations with a thickness of greater than 38 km, our H_n measurements, which were also obtained by assuming that $\phi = 1.73$, are systematically smaller than those obtained by Nguuri et al. with a difference of several kilometers. This difference is caused by the fact that for crust thicker than 38 km, the portion of the crust below 38 km is assigned a mantle velocity, rather than a crustal velocity, which leads to an overestimation of the thickness. Given that crust-mantle velocity contrast is large, about 20%, this effect is significant. Results presented in

Table 2. Regional Averages of Crustal Thickness (H), $V_p/V_s(\phi)$ and R

Area	Mean H, km	Mean ϕ	Mean R	Number of Stations
A	37.8 ± 0.9	1.732 ± 0.017	0.135 ± 0.027	7
B	48.1 ± 3.6	−	0.070 ± 0.013	5
C	43.5 ± 4.4	1.739 ± 0.010	0.132 ± 0.048	10
D	43.4 ± 3.7	1.775 ± 0.031	0.112 ± 0.035	19
E	37.4 ± 1.8	1.731 ± 0.024	0.176 ± 0.062	27
F	44.7 ± 5.5	1.720 ± 0.016	0.145 ± 0.062	14
All	41.4 ± 4.9	1.740 ± 0.029	0.141 ± 0.058	82
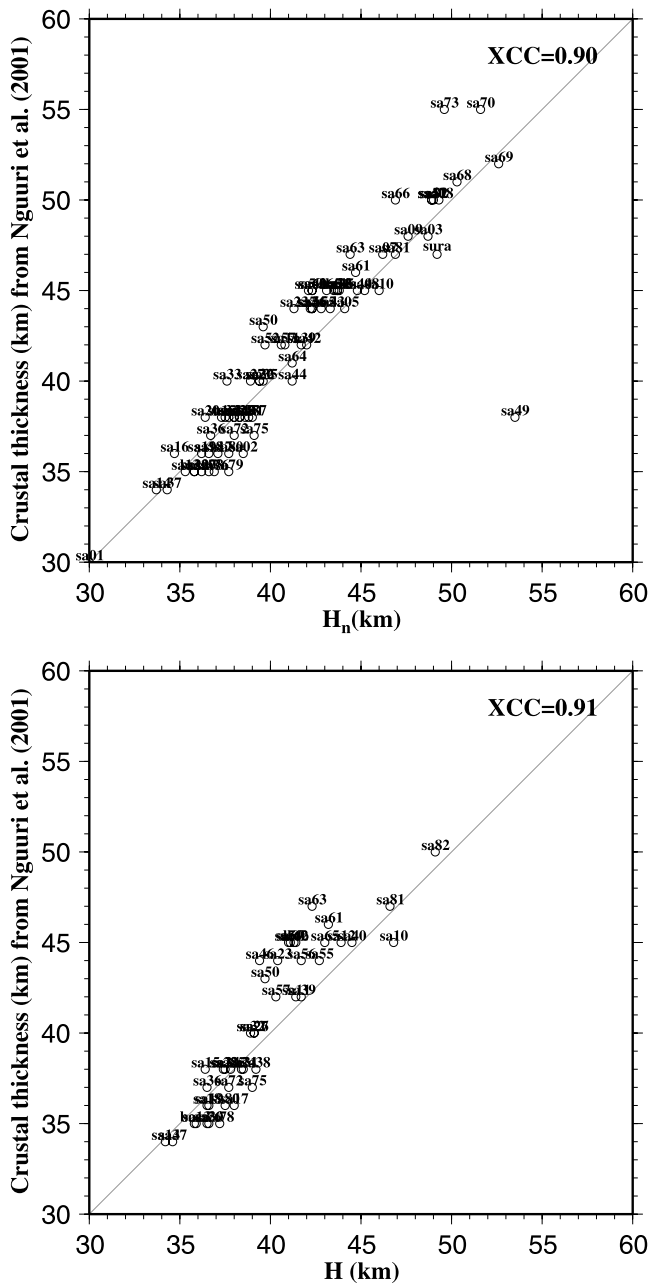
Figure 12. Comparison of crustal thickness measurements obtained by this study and those by *Nguuri et al.* [2001]. (top) Crustal thicknesses obtained using a fixed ϕ = 1.73, and (bottom) crustal thicknesses obtained by searching for the optimal pair of (H, ϕ).

this study were obtained using crustal velocities above the Moho regardless of its actual thickness.

[46] Finally, the largest discrepancy (38 vs. 54 km) between the two data sets is found at sa49, and this is due to the weakness of the $P\acute{m}S$ phases. We note that our result (54 km) is more consistent with nearby stations.

5.2. Spatial Distribution of ϕ

[47] The spatial variations in ϕ are remarkably coherent throughout southern Africa, with the southern Kaapvaal and eastern Zimbabwe cratons showing the lowest values, and

the Bushveld region showing the highest. The collisional belts of the Limpopo and Namaqua-Natal show values of ϕ that are similar to but more spatially variable than the cratons. The resulting ϕ values have no obvious relationship with either crustal thickness or the age of the surface rocks (Figures 1 and 10). The regions of thickened crust, namely, Limpopo, Bushveld and Namaqua-Natal show a wide range of ϕ values. The only apparent relationship is that the thinnest crust in the southern part of the Kaapvaal craton also possesses the smallest ϕ. Similarly there is no obvious age relationship to ϕ, as there is no significant difference in ϕ between on-craton and off-craton regions. A histogram (Figure 13) of all of the ϕ measurements suggests that overall, the measurements in the Bushveld are significantly larger (mean of 1.78) than those in the other areas (mean of 1.74). As noted previously and indicated by the histogram, the most prominent characteristic of the data set is that the highest values for ϕ are found in the vicinity of the Bushveld. The study that most closely parallels the present one, based on both methodology and geology of terrains examined, is the analysis of the Australian continent by *Chevrot and van der Hilst* [2000]. As in our case, they find no simple relationship between ϕ and H or between ϕ and crustal age. They observe a distinct subset of their measurements that have very high values of ϕ (1.80 or above) that span the entire range of ages and crustal thicknesses.

[48] There have been a variety of other studies of ϕ, as noted in the introduction, such as *Zandt and Ammon* [1995], that suggest increasing ϕ with age. Our results are clearly inconsistent with this observation. The uncertainties in that study, however, were so large that they cover roughly our entire range of estimates, from 1.70 to 1.82.

[49] The mean ϕ value (1.74) obtained in this study is also lower than several previous studies. For example, *Zandt and Ammon* [1995] obtained an average value of 1.81 ± 0.04 for shields and platforms, while *Chevrot and van der Hilst* [2000] obtained an average value of 1.76 ± 0.01.

5.3. Composition of the Cratonic Crust

[50] We now seek to use our crustal parameters to constrain both the composition and evolution of the southern African crust. Because numerous previous petrological studies suggest that the upper continental crust is felsic, we can use our estimates of ϕ to constrain lower crustal composition. In this study we use the classification of lower crustal rocks of *Holbrook et al.* [1992], who consider rocks
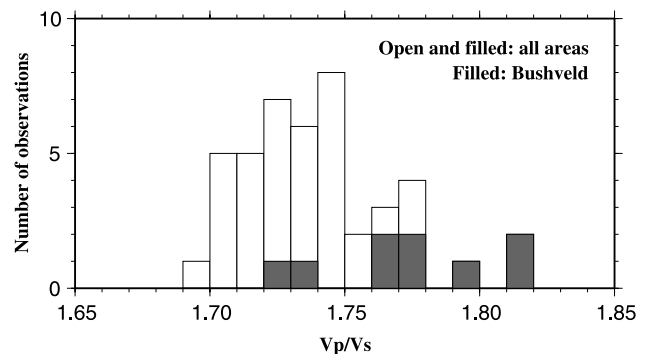
Figure 13. Histogram of ϕ.

with a ϕ of 1.76 or smaller as being felsic, between 1.76 and 1.81 as intermediate, and larger than 1.81 as mafic.

[51] It is useful to compare our results with the petrologic crustal model of *Christensen and Mooney* [1995]. They constructed an average *P* velocity profile for the crust, based on an extensive compilation of seismic studies, and then used these, in conjunction with laboratory measurements of *P* wave velocity, to construct a petrologic model. That model has subsequently been converted to ϕ using the laboratory velocity measurements of *Christensen* [1996]. This model ranges from a ϕ of 1.74 in the upper crust to 1.81 in the lower crust, with an average value of 1.78. Our average value of 1.74 is thus significantly lower than this average value, and corresponds to an approximately 5% increase in SiO2 content [*Christensen*, 1996]. If we assume that the Christensen model is correct for the upper crust, namely, that it is felsic, then the lower crust beneath southern Africa is significantly less mafic than this average composition. Another line of evidence supporting a more felsic lower crust has to do with the expected effect of collisional deformation. Such deformation will lead to crustal thickening, uplift, and ultimately erosion of the top layer. If this top layer is less mafic than the crust as a whole, then erosion will tend to increase ϕ. Alternatively, if the upper and lower crust have similar compositions, then this process will have little to no effect on ϕ. Since we do not observe a significant increase in ϕ in the collisional zones, compared to the more stable part of the craton, it suggests that the upper and lower crust have the same felsic composition.

5.4. Crustal Modification by the Bushveld Event

[52] It is reasonable to hypothesize that the high ϕ and H values observed in the vicinity of the Bushveld are due to basalt intruding the crust from the mantle below. Under the assumption that the crust is isostatically compensated, it is possible to solve for the thickness of the mafic layer, and to estimate the value of ϕ for this layer to check whether it is consistent with a mafic composition. Assuming the density of such a layer is 3000 kg/m^3 versus 3300 kg/m^3 for the mantle and 2700 kg/m^3 for the rest of the crust, then given the difference of 6 km in crustal thickness between region *E* (taken to be normal crust) and *D* (taken to consist of normal crust plus the mafic layer), the thickness of the mafic layer, H_{mafic}, is estimated to be about 12 km. If we take this thickness and assume that the normal crust has the same value of ϕ as beneath region *E*, ϕ_E, then ϕ_{mafic} can be obtained using $H_{mafic} \phi_{mafic} + H_E * \phi_E = (H_{mafic} + H_E)\phi_D$, where ϕ_D is the observed mean ϕ value for region *D* (1.77) and H_E is the thickness of region *E*-type crust in region *D* ($H_D - H_{mafic}$). Taking $\phi_E = 1.73$, the resulting ϕ_{mafic} is 1.87 which is very consistent with a mafic composition. Thus a mafic layer successfully accounts for both the thickness and V_P/V_S ratio variations between the Bushveld region and the rest of the study area. In addition, the presence of a mafic layer near the Moho and the disruption caused by the intrusion process itself could also account for the small *R* values observed in the vicinity of the Complex.

[53] As we have noted above, the zone of high ϕ in region *D* is significantly larger than the surface extent of the Bushveld intrusion. In particular, it extends several hundred kilometers to the west and about 100 km to the north of

observed outcrops. Yet, the success of our simple mafic intrusion model in accounting for the seismic properties suggests that the intrusion may simply have a larger lateral extent in the crust than what is observed as outcrop at the surface. Indeed, there is evidence supporting this larger size. The most western stations with large ϕ are close to the Molopo Farms Complex (Figure 10), which is a mafic intrusion that has virtually the same age as the Bushveld [*Cawthorn and Walraven*, 1998]. While there is debate whether these two intrusions are connected at depth, their identical age, and the fact that the same structure (TML, the Thabazimbi-Murchison Lineament) is implicated in both (Figure 1), suggest that this is a very reasonable conclusion and is consistent with our results. Regarding a possible northward extension of the Bushveld, we note that the most northern outcrop of the Bushveld, Villa Nora (near station sa51), is about 100 km north of the main lobes and thus roughly at the same latitude of the most northern stations (e.g., sa63) that possess large values of ϕ. We hypothesize that the basaltic intrusions in the crust extend in roughly a rectangular region, bounded by Molopo Farms to the west and Villa Nora to the north (Figure 10).

5.5. Crustal Evolution

[54] The basic result of our study is that the values of ϕ are low and fairly uniform, with the notable exception of the high values associated with Bushveld intrusion. As we have noted, the high Bushveld values likely represent the subsequent addition of a mafic component, rather than variability that was present since the formation of the crust. The low values of ϕ elsewhere, and their apparent age independence place important constraints on models for crustal formation and evolution. As is well known, there is a fundamental problem with the leading model of continental crustal formation from island arc magmatism, specifically that arc crust appears to be more mafic than continental crust, thus giving rise to a long-standing paradox [*Rudnick*, 1995; *Kelemen*, 1995]. In many ways, our results serve to accentuate this paradox, in that they highlight the role of subsequent mafic intrusions (and flood basalts) in rendering the overall composition of continental crust more mafic than when it first formed. Within the context of this island arc mechanism for creating continental crust, there have been a variety of proposed ways of resolving this paradox. (1) In the Archean, the subducted basaltic oceanic crust is melted to produce a felsic composition, and the residue is then subducted. (2) The composition of the continental crust is indeed mafic, consisting of a felsic upper crust and mafic-to-ultramafic residue residing in the lower crust and that this upper crust/lower crust boundary has been misinterpreted by seismologists as the Moho separating the crust and mantle. (3) The residue is dense and delaminates, leaving only the felsic component. We consider these possibilities within the context of our results.

5.5.1. Age Dependence of Crustal Composition

[55] Regarding (1) above, it has been argued that the higher mantle temperatures in the Archean produced more felsic compositions through partial melting of subducted oceanic crust [*Martin*, 1986; *Drummond and Defant*, 1990], rather than the peridotitic upper mantle that is expected to produce a more mafic composition. As mantle temperatures decrease over time, slab melting ceases, thus predicting more

mafic melts for younger ages. If slab melting were the dominant crust-forming process, then such a model would predict that older continental crust should be more felsic in composition than younger crust. As we have noted, however, no such systematic age variation is observed (Figure 10), nor is it observed in Australia [*Chevrot and van der Hilst*, 2000]. Thus our data do not support this mechanism.

5.5.2. Hidden Residue

[56] It has also been argued that the lower crust has been transformed to dense, seismically fast mafic-to-ultramafic assemblages [*Kay and Kay*, 1985], which are therefore seismically indistinguishable from the mantle material. Under this model, the seismic Moho is the boundary between the felsic upper crust and the mafic lower crust, whereas the petrological Moho between the crust and mantle would not be seismically observable. While such a model is permitted by the seismic observations, it cannot explain the paucity of such lower crustal xenoliths in the study area [*Schulze*, 1989]. Indeed, by volume, this mafic/ultramafic residue should be several times the volume of the felsic crust, in which case most of the subcontinental lithospheric "mantle" should be composed of this material. Clearly basalt-depleted peridotites dominate the distribution of xenoliths coming from depths greater than the "seismic Moho".

5.5.3. Crustal Delamination: Constraining Its Timing and Environment

[57] We are then left with the third possibility of resolving the paradox, namely, that the dense mafic/ultramafic residue from the partial melting of basalt is removed from the crust by delamination, as advocated by several authors [*Arndt and Goldstein*, 1989; *Kay and Kay*, 1991; *Nelson*, 1991; *Gao et al.*, 1998; *Meissner and Mooney*, 1998; *Jull and Kelemen*, 2001]. Within the context of this process, we seek to constrain the possible environment and timing of delamination. As discussed by *Jull and Kelemen* [2001], crustal delamination is unlikely to occur in low-temperature environments, such as stable cratons because viscosity of the subcontinental mantle is too high. Thus crustal delamination would require delamination of the underlying lithospheric mantle as well [*Rudnick*, 1995]. There is overwhelming evidence in the regions sampled by mantle xenoliths in southern Africa, and indeed globally, that mantle delamination rarely occurs in cratonic environments [*Silver et al.*, 2004, 2006]. Therefore crustal delamination must precede the stabilization of continental lithosphere. Of the possible high-temperature environments, *Jull and Kelemen* [2001] suggest that crustal delamination should be restricted to arcs, volcanic rifted margins, continental regions undergoing extension, regions underlain by a mantle plume, or zones that have undergone mantle delamination. All but the first of these represent environments that are distinctly separated from the assumed region of crust formation, at island arcs. If the uniformity in felsic composition that we infer is more generally true of continents, it then requires that there be a close spatial and temporal linkage between the crust formation and crustal delamination processes. Otherwise, we would observe many regions where delamination has not occurred, thereby yielding values of φ that are on-average mafic in composition. This is not observed.

[58] The simplest way to always produce a felsic crust from arc magmatism is if delamination is synchronous with the partial melting of basalt. This makes a simple prediction, then, that values of φ for mature arcs should be approximately the same as the "felsic" values for southern Africa. The presently available data on φ, however, suggest that they are higher (more mafic) than continental crust. For example, *Holbrook et al.* [1999] concluded that the Aleutian arc is on-average mafic in composition. If this is a general feature of arcs, then delamination must postdate the island arc formation stage. The next stage that is required for island arcs to ultimately become continents is the docking of the arc to a continental margin. Indeed, several groups have proposed this idea [*Holbrook et al.*, 1999; *Draut et al.*, 2002]. If this is indeed a general feature, then delamination is restricted to have occurred after the formation of the arc, but before lithospheric stabilization. The only difficulty with invoking delamination at this time is that it also requires removal of the lithospheric mantle portion of the protocontinent. We note that the leading model for the formation of cratons is the collision-induced advective thickening of preexisting island arc lithospheric fragments. It thus becomes difficult to reconcile the need for crustal delamination with the preservation and indeed thickening of the lithospheric process, through the orogenic process.

5.5.4. Proposed Tests

[59] This study suggests several lines of research that follow directly from our study of southern Africa. First, it would be important to determine to what extent flood basalts increase the value of φ in a way that is similar to what we find for the Bushveld in southern Africa. If there is a systematic effect, then it suggests that continental crust, when formed, is even more felsic than presently thought. Second, it would be worthwhile to conduct a systematic global study of φ for island arcs, to place the island arc/continental crust paradox on a more quantitative basis. Finally, if indeed delamination occurs during the collision of an arc with an existing continent, then it should be possible to test this possibility in recently accreted terrains.

6. Conclusions

[60] Several conclusions can be drawn from the study:

[61] 1. Outside of the Bushveld region, the crust of southern Africa is characterized by low values of φ, suggesting a felsic upper and lower crust.

[62] 2. The largest φ values are associated spatially with the Bushveld Complex, and is most likely due to the intrusion of basalt into the crust. The addition of basaltic material successfully explains the thicker crust, in terms of isostatic compensation, higher φ, as well as the diffuse character of the Moho in this area. We suggest that mafic addition is a dominant process in the modification of crustal composition.

[63] 3. We find that collisional zones, such as the Limpopo belt, have values of φ that are not significantly different from surrounding regions. Because such collisions are expected, through erosion of the top layer, to make the crust more mafic (if the lower crust is more mafic than the upper crust), we infer that the upper and lower crust are similar in composition in this region.

[64] 4. The simplest model consistent with our data is that the crust beneath southern Africa possesses a roughly

uniform felsic composition, approximately unchanged since soon after its formation, and that crust that is observed to be more mafic is due to the addition of basalt to the crust, rather than the failure of mafic melt residue to delaminate.

References

Ammon, C. J., G. E. Randall, and G. Zandt (1990), On the non-uniqueness of receiver function inversions, *J. Geophys. Res.*, *95*, 15,303–15,318.

Arndt, N. T., and S. L. Goldstein (1989), An open boundary between lower continental crust and mantle: its role in crust formation and crustal recycling, *Tectonophysics*, *161*, 201–212.

Braile, L. W., W. J. Hinze, R. R. B. von Frese, and G. R. Keller (1989), Seismic properties of the crust and uppermost mantle of the conterminous United States and adjacent Canada, in *Geophysical Framework of the Continental United States*, edited by L. C. Pakiser and W. D. Mooney, *Mem. Geol. Soc. Am.*, *172*, 655–680.

Cawthorn, R. G., and F. Walraven (1998), Emplacement and crystallization time for the Bushveld Complex, *J. Petrol.*, *39*, 1669–1687.

Chevrot, S., and R. D. van der Hilst (2000), The Poisson ratio of the Australian crust: Geological and geophysical implications, *Earth Planet. Sci. Lett.*, *183*, 121–132.

Christensen, N. I. (1996), Poisson's ratio and crustal seismology, *J. Geophys. Res.*, *101*, 3139–3156.

Christensen, N. I., and W. D. Mooney (1995), Seismic velocity structure and composition of the continental crust: A global view, *J. Geophys. Res.*, *100*, 9761–9788.

Clarke, T. J., and P. G. Silver (1991), A procedure for the systematic interpretation of body wave seismograms. 1. Application to Moho depth and crustal properties, *Geophys. J. Int.*, *104*, 41–72.

Clarke, T. J., and P. G. Silver (1993), Estimation of crustal Poisson's ratio from broad band teleseismic data, *Geophys. Res. Lett.*, *20*, 241–244.

de Beer, J. H., and E. H. Stettler (1988), Geophysical characteristics of the southern African continental crust, *J. Petrol., Spec. Vol.*, 163–184.

de Wit, M. J., and C. Roering (1990), The Limpopo Belt, in *A Field Workshop on Granulites and Deep Crustal Tectonics, Extended Abstracts*, edited by J. M. Barton, pp. 42–52, Rand Afrikaans Univ., Johannesburg.

de Wit, M. J., C. Roering, R. J. Hart, R. A. Armstrong, C. E. J. de Ronde, R. W. E. Green, M. Tredoux, E. Peberdy, and R. A. Hart (1992), Formation of an Archean continent, *Nature*, *357*, 553–562.

Draut, A. E., P. D. Clift, R. E. Hannigan, G. Layne, and N. Shimizu (2002), A model for continental crust genesis by arc accretion: rare earth element evidence from the Irish Caledonides, *Earth Planet. Sci. Lett.*, *203*, 861–877.

Drummond, M. S., and M. J. Defant (1990), A model for trondhjemite-tonalite-dacite genesis and crustal growth via slab melting: Archean to modern comparisons, *J. Geophys. Res.*, *95*, 21,503–21,521.

Dueker, K. G., and A. F. Sheehan (1998), Mantle discontinuity structure beneath the Colorado Rocky Mountains and High Plains, *J. Geophys. Res.*, *103*, 7153–7169.

Durrheim, R. J., and R. W. Green (1992), A seismic refraction investigation of the Archaean Kaapvaal Craton, South Africa, using mine tremors as the energy source, *Geophys. J. Int.*, *108*, 812–832.

Durrheim, R. J., and W. D. Mooney (1994), Evolution of the Precambrian lithosphere: Seismological and geochemical constraints, *J. Geophys. Res.*, *99*, 15,359–15,374.

Efron, B., and R. Tibshirani (1986), Bootstrap methods for standard errors, confidence intervals, and other measures of statistical accuracy, *Stat. Sci.*, *1*, 54–77.

Egorkin, A. (1998), Velocity structure, composition and discrimination of crustal provinces in the former Soviet Union, *Tectonophysics*, *298*, 395–404.

Freybourger, M., J. B. Gaherty, T. H. Jordan, and the Kaapvaal Seismic Group (2001), Structure of the Kaapvaal craton from surface waves, *Geophys. Res. Lett.*, *28*, 2489–2492.

Gao, S., B. R. Zhang, Z. M. Jin, H. Kern, T. C. Luo, and Z. D. Zhao (1998), How mafic is the lower continental crust?, *Earth Plant. Sci. Lett.*, *106*, 101–117.

Gao, S. S., P. G. Silver, K. H. Liu, and Kaapvaal Seismic Group (2002), Mantle discontinuities beneath Southern Africa, *Geophys. Res. Lett.*, *29*(10), 1491, doi:10.1029/2001GL013834.

Griffin, W. L., and S. Y. O'Reilly (1987), Is the continental *Moho* the crust-mantle boundary?, *Geology*, *15*, 241–244.

Holbrook, W. S., W. D. Mooney, and N. I. Christensen (1992), The seismic velocity structure of the deep continental crust, in *Continental Lower Crust*, edited by D. M. Fountain, R. Arculus, and R. W. Kay, pp. 21–43, Elsevier, New York.

Holbrook, W. S., D. Lizarralde, S. McGeary, N. Bangs, and J. Diebold (1999), Structure and composition of the Aleutian island arc and implications for continental crustal growth, *Geology*, *27*, 31–34.

James, D. E., M. J. Fouch, J. C. VanDecar, S. van der Lee, and the Kaapvaal Seismic Group (2001), Tectospheric structure beneath southern Africa, *Geophys. Res. Lett.*, *28*, 2485–2488.

Jull, M., and P. B. Kelemen (2001), On the conditions for lower crustal convective instability, *J. Geophys. Res.*, *106*, 6423–6446.

Kay, S. M., and R. W. Kay (1985), Role of crustal cummulates and the oceanic crust in the formation of the lower crust of the Archean arc, *Geology*, *13*, 461–464.

Kay, R. W., and S. M. Kay (1991), Creation and destruction of lower continental crust, *Geol. Rundsch.*, *80*, 207–223.

Kelemen, P. B. (1995), Genesis of high Mg# andesites and the continental crust, *Contrib. Mineral. Petrol.*, *20*(1), 1–19.

Kennett, B. L. N., and E. R. Engdahl (1991), Traveltimes for global earthquake location and phase identification, *Geophys. J. Int.*, *105*, 429–465.

Kind, R., X. Yuan, J. Saul, D. Nelson, S. V. Sobolev, J. Mechie, W. Zhao, G. Kosarev, J. Ni, U. Achauer, and M. Jiang (2002), Seismic images of crust and upper mantle beneath Tibet: Evidence for Eurasian plate subduction, *Science*, *298*, 1219–1221.

Martin, H. (1986), Effects of steeper Archean geothermal gradient on geochemistry and subduction-zone magmas, *Geology*, *14*, 753–756.

Meissner, R., and W. Mooney (1998), Weakness of the lower continental crust: A condition for delamination, uplift, and escape, *Tectonophysics*, *296*, 47–60.

Nelson, K. D. (1991), A unified view of cratonic evolution motivated by recent deep seismic reflection and refraction results, *Geophys. J. Int.*, *105*, 25–35.

Nguuri, T. K., J. Gore, D. E. James, S. J. Webb, and Kaapvaal Seismic Group (2001), Crustal structure beneath southern Africa and its implications for the formation and evolution of the Kaapvaal and Zimbabwe cratons, *Geophys. Res. Lett.*, *28*, 2501–2504.

Niu, F. L., and D. E. James (2002), Fine structure of the lowermost crust beneath the Kaapvaal craton and its implications for crustal formation and evolution, *Earth Planet. Sci. Lett.*, *200*, 121–130.

Niu, F. L., A. Levander, C. M. Cooper, C. A. Lee, A. Lenardic, and D. E. James (2004), Seismic constraints on the depth and composition of the mantle keel beneath the Kaapvaal craton, *Earth Planet. Sci. Lett.*, *224*, 337–346.

Owens, T. J., and G. Zandt (1997), Implications of crustal property variations for models of Tibetan Plateau evolution, *Nature*, *387*, 37–43.

Press, W. H., S. A. Teukolsky, W. T. Vetterling, and B. P. Flannery (1992), *Numerical Recipes in FORTRAN*, 2nd ed., Cambridge Univ. Press, New York.

Ranganai, R. T., A. B. Kampunzu, E. A. Atekwana, B. K. Paya, J. G. King, D. I. Koosimile, and E. H. Stettler (2002), Gravity evidence for a larger Limpopo Belt in southern Africa and geodynamic implications, *Geophys. J. Int.*, *149*, F9–F14.

Rudnick, R. L. (1995), Making continental crust, *Nature*, *378*, 571–578.

Rudnick, R. L., and D. M. Fountain (1995), Nature and composition of the continental crust: A lower crustal perspective, *Rev. Geophys.*, *33*, 267–309.

Schulze, D. J. (1989), Constraints on the abundance of eclogite in the upper mantle, *J. Geophys. Res.*, *94*, 4205–4212.

Shen, Y., and J. Blum (2003), Seismic evidence for accumulated oceanic crust above the 660-km discontinuity beneath southern Africa, *Geophys. Res. Lett.*, *30*(18), 1925, doi:10.1029/2003GL017991.

Sheriff, R. E., and L. P. Geldart (1993), *Exploration Seismology*, 2nd ed., Cambridge Univ. Press, New York.

Silver, P. G., S. S. Gao, K. H. Liu, and The Kaapvaal Seismic Group (2001), Mantle deformation beneath southern Africa, *Geophys. Res. Lett.*, *28*, 2493–2496.

Silver, P. G., M. Fouch, S. S. Gao, M. D. Schmitz, and the Kaapvaal Seismic Group (2004), Seismic anisotropy, mantle fabric, and the magmatic evolution of Precambrian southern Africa, *S. Afr. J. Geol.*, *107*, 47–60.

Silver, P. G., M. Behn, K. Kelley, M. Schmitz, and B. Savage (2006), Understanding cratonic flood basalts, *Earth Planet. Sci. Lett.*, in press.

Stankiewicz, J., S. Chevrot, R. D. van der Hilst, and M. J. de Wit (2002), Crustal thickness, discontinuity depth, and upper mantle structure beneath southern Africa: Constraints from body wave conversion, *Phys. Earth Planet. Inter.*, *130*, 235–251.

Tankard, A. J., M. P. Jackson, K. A. Eriksson, D. K. Hobday, D. R. Hunter, and W. E. Minter (1982), *Crustal Evolution of Southern Africa: 3.8 Billion Years of Earth History*, Springer, New York.

Tarkov, A. P., and V. V. Vavakin (1982), Poisson's ratio behavior in various crystalline rocks: Application to the study of the Earth's interior, *Phys. Earth Planet. Inter.*, *29*, 24–29.

Webb, S. J., R. G. Cawthorn, T. Nguuri, and D. James (2004), Gravity modeling of Bushveld Complex connectivity supported by Southern African Seismic Experiment results, *S. Afr. J. Geol.*, *107*, 207–218.

Zandt, G., and C. J. Ammon (1995), Continental-crust composition constrained by measurements of crustal Poisson's ratio, *Nature*, *374*, 152–154.

Zandt, G., S. C. Myers, and T. C. Wallace (1995), Crust and mantle structure across the Basin and Range–Colorado plateau boundary at 37°N latitude and implications for Cenozoic extensional mechanism, *J. Geophys. Res.*, *100*, 10,529–10,548.

Zhu, L. P., and H. Kanamori (2000), Moho depth variation in southern California from teleseismic receiver functions, *J. Geophys. Res.*, *105*, 2969–2980.

————————————

S. S. Gao, K. H. Liu, and S. K. Nair, Geophysics Group, 108 Thompson Hall, Kansas State University, Manhattan, KS 66506, USA. (gao@ksu.edu; liu@ksu.edu; snair@ksu.edu)

P. G. Silver, Department of Terrestrial Magnetism, Carnegie Institution of Washington, 5241 Broad Branch Road, N.W., Washington, DC 20015, USA. (silver@dtm.ciw.edu)